Transportation Geotechnics 21 (2019) 100276

Contents lists available at ScienceDirect

Transportation Geotechnics

journal homepage: www.elsevier.com/locate/trgeo

Dynamic properties of lightweight foamed glass and their effect on railway vibration

Stanislav Lenart[a,*], Amir M. Kaynia[b]

[a] Slovenian National Building and Civil Engineering Institute (ZAG), Dimičeva ulica 12, Ljubljana, Slovenia
[b] Norwegian Geotechnical Institute (NGI), PO Box 3930 Ullevaal Stadion, N-0806 Oslo, Norway

ARTICLE INFO

Keywords:
Lightweight material
Recycled foamed glass
Railway vibration
Shear modulus
Damping

ABSTRACT

Deformation properties of lightweight coarse grained material from recycled foamed glass have been determined from large-scale triaxial tests on prismatic specimens with dimensions 40 cm × 40 cm × 80 cm. Deformations were measured locally using vertical and horizontal local deformation transducers. Monotonic and cyclic loading at small to medium strain range were conducted. Three load sequences representing the expected conditions of use of lightweight material as vibration-reducing material in railway geotechnics have been used. Results indicate strong effect of brittle cellular structure of tested material as well as confining pressure dependency of elastic threshold shear strain and damping ratio. The results were used to assess the applicability of empirical formulas for shear modulus of granular materials to lightweight foamed glass. The parameters determined from the laboratory tests were further used in numerical analysis of railway dynamic response. The results of the numerical simulations show that replacement of fill in track embankment by lightweight material could improve the dynamic response of the track in reducing the vibration.

Introduction

Civil engineering and infrastructure applications on compressible and low-strength subgrade presents construction challenges. Particularly, when significant time to complete primary consolidation settlements is required, innovative construction approaches are needed. Various soil improvements techniques, e.g. lime cement columns, are sometimes costly and do not perform as desired, and in addition, they may present other challenges. An alternative solution is the use of lightweight fill materials [10,24]. The common characteristic of these materials is their high porosity with continuous or discontinuous pores. Among the most commonly used lightweight materials in earthworks are expanded polystyrene (EPS) [6,39,10,28], extruded polystyrene (XPS) boards [13], granulated tire rubber [26,33,31] and various natural and artificial lightweight aggregates (LWA), e.g. lightweight clay aggregate [13,5], LWA from sand sludge [37], and foam glass aggregate [40,29].

Due to low density, use of LWA can represent an added advantage in lightweight foam concretes used as subgrade bed filler in railway tracks [12], where the primary reason for the use of these aggregates is weight reduction. However, LWA can also be used without any binder as a raw aggregate in various applications. Dense closed pores in LWA enable good thermal properties of such materials [7], offering frost resistive alternative to natural gravel or crushed rock material as main aggregates in base, sub-base and frost protection layers in cold regions [21]. Particularly in Nordic countries, LWA has been used in several applications in a number of projects over the last decades for insulation purposes, reducing settlements and improving stability of fills on soft subsoil [38]. The pore walls in LWA are relatively thick as compared with the diameter of the voids, which gives the aggregates fairly high compressive strengths [7]. Therefore, despite being light weight, LWA could offer considerable stiffness.

This paper focuses on recycled foamed glass aggregate as a LWA, and its utilization in small strain range for dynamic loading applications where the elastic characteristics govern the response. Therefore, quasi-elastic properties of recycled foamed glass are of most interest in this paper. The effect of different pore sizes on the strength of foamed glass has already been shown [30], and Kurachi et al. [17] has explained the mechanism of high energy absorption by foamed glass aggregate. Arulrajah et al. [4] presented basic engineering and environmental properties of this material, highlighting high shear resistance at large displacements and non-hazardous characteristic. It is stated in Arulrajah et al. [4] that all hazardous concentrations in the leachate are far lower than 100 times of those of the drinking water standards. All these properties make the lightweight recycled foamed glass aggregate desirable for bulk use in earthworks, utilized as a lightweight fill and

* Corresponding author.
E-mail addresses: stanislav.lenart@zag.si (S. Lenart), amir.m.kaynia@ngi.no (A.M. Kaynia).

https://doi.org/10.1016/j.trgeo.2019.100276
Received 21 May 2019; Received in revised form 25 August 2019; Accepted 28 August 2019
Available online 29 August 2019

ground improvement material [22].

Basic engineering properties of recycled foamed glass aggregate such as CBR, apparent cohesion and friction angle have already been studied (e.g. [4]), while there is a lack of information on deformation properties of this material, particularly damping and stiffness at small strains. Thus, the first part of this paper presents laboratory testing and interpretation of these properties. Possible use of lightweight recycled foamed glass aggregate in the embankment of railway track is illustrated by numerical simulations in the second part of the paper. It is emphasized that it is not the intention of this study to promote lightweight foamed glass aggregate as replacement for ballast/sub-ballast. Considering the brittle nature of foamed glass aggregate, specialized/standardized tests are required to evaluate their suitability for such usage. This evaluation is outside of the scope of the present study.

Material and testing procedure

Lightweight material

Lightweight coarse grained material from recycled foamed glass was tested in this research. The material was obtained from Norwegian manufacturer Glasopor AS, which produce this cellular glass aggregate from recycled glass containers collected from households. The glass is milled to glass powder and then expanded at high temperatures broken by cooling. The outcome of the production process is a granular material of aggregate size 10–60 mm with dry bulk density of just 180 kg/m^3. The product can be used as thermal insulation or as lightweight fill material.

Results of sieve analysis performed on the tested material and typical grains are presented on Fig. 1. One can observe a narrow gradation with aggregate of approximately the same size with a coefficient of uniformity C_u = 1.6. Approximately 80% of the angular particles are between 30 mm and 60 mm size. The tested material contained almost no fine aggregate particles, which results in a large void ratio. Besides air voids between particles, cellular structure of aggregate with air voids within the grains is typical for recycled foamed glass. These characteristics result in very low bulk density and specific gravity G_s equal to only 3.60 kN/m^3. Key engineering parameters of the tested material are listed in Table 1.

A series of vacuum tests on prismatic specimens with height 80 cm and cross section 40 × 40 cm was conducted for this study (Fig. 2). Several tests were carried out in advance in order to ensure satisfactory testing procedure according to the extreme loading and measurement

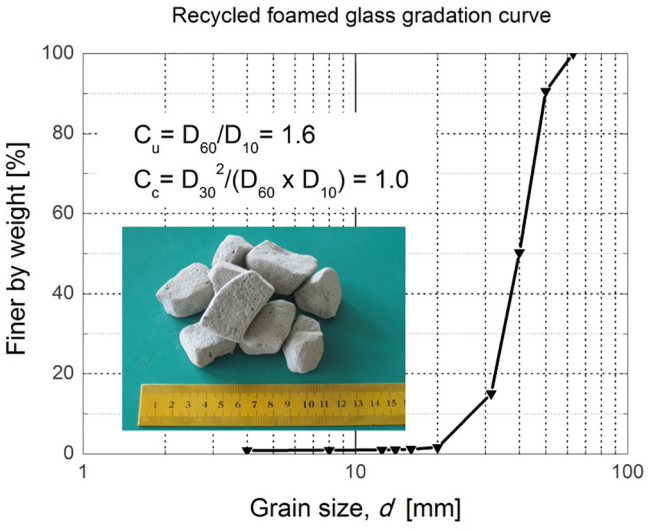

Fig. 1. Grain size distribution of the tested lightweight material from recycled foamed glass.

Table 1
Key material properties of tested recycled foamed glass.

Grain size, d	[mm]	10–60
Dry density, ρ	[kg/m^3]	240*
Specific gravity, G_s	[–]	0.36
Resistance to crushing	[kPa]	770**
Friction angle, ϕ	[°]	45

* Gravity compacted samples.
** Value reported by manufacturer [9].

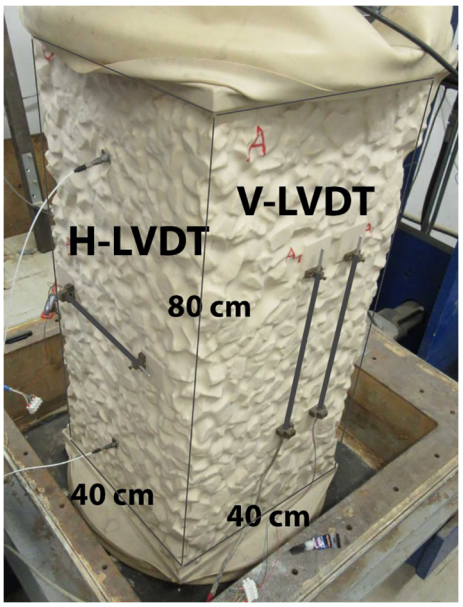

Fig. 2. Prismatic specimen with local linear variable displacement transducers (LVDTs).

accuracy requirements. Results of the last tests, which achieved the highest accuracy, are presented in this paper.

For preparation of the test specimens, the material was lightly compacted manually in several layers to achieve the desired density typical for normal use in the field. In any case, heavy compaction of tested coarse grained material is difficult due to very uniform gradation.

Large-scale triaxial apparatus

The large-scale triaxial apparatus at the Slovenian National Building and Civil Engineering Institute (ZAG) was used in this study. Conventionally, confining pressure is applied on specimen by the fluid contained within the triaxial cell, through a rubber membrane surrounding the specimen [25]. Because the largest grain size that can be accurately examined in the triaxial apparatus should not exceed about one-sixth of the diameter of the testing specimen [35], testing large grain-size would require very large triaxial cell. On the other hand, only low to moderate confining pressures have been of interest in this study because of the envisaged use of the material (i.e. dynamics and vibration related). This material is supposed to be used relatively close to the surface where the confinement is not expected to exceed 100 kPa. Therefore, the confining pressure was applied by means of a partial vacuum, as back pressure, as also performed by others [35,20,8]. The procedures described in previous studies (e.g. [1,20]) were used for calibration of the transducers. The test results were validated by test repetitions.

The axial loading device employs an electro-hydraulic actuator with a capacity of 100 kN. The axial load is measured by means of two load cells attached successively at the top cap, in order to eliminate the

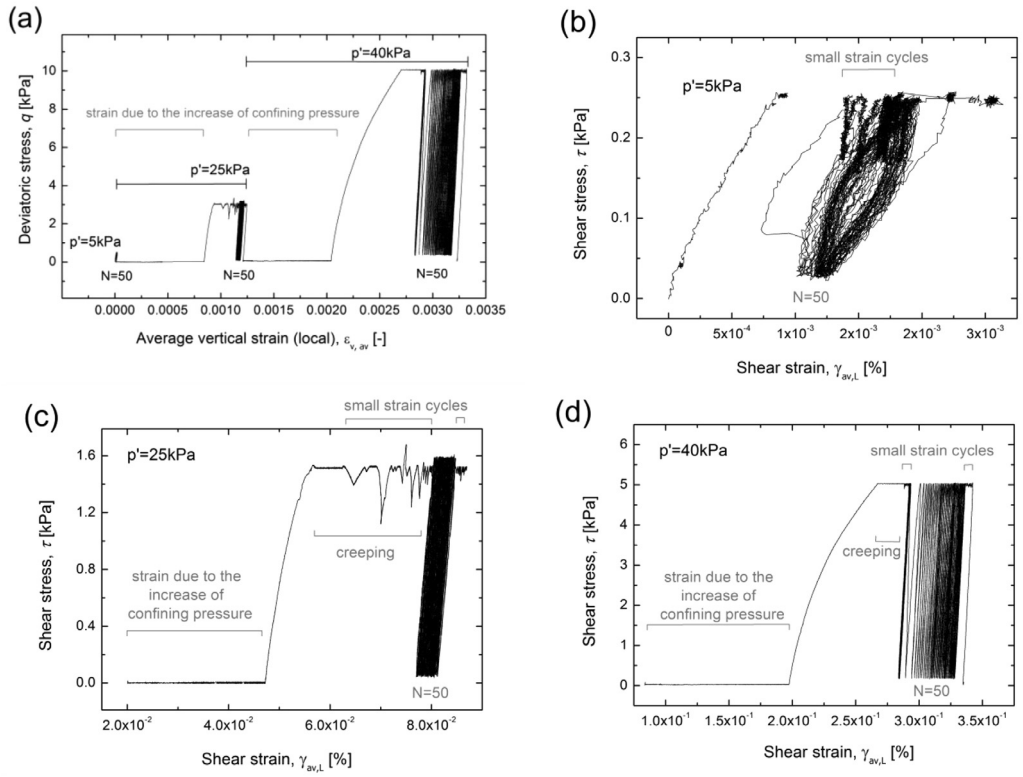

Fig. 3. The course of testing procedure: (a) overall stress path in test, and shear-stress vs. shear strain for confining pressure, (b) p′ = 5 kPa, (c) p′ = 25 kPa and (d) p′ = 40 kPa.

effects of piston friction. The load cells have different capacities. The first one (with higher accuracy) was used for measurements within low load range (up to 10 kN), while the other one was used over this range. The first load cell is mechanically protected such that when the load exceeds its range, the measurements are performed by the second one.

Axial strains (ε_v) were measured by a pair of linear variable displacement transducers (LVDTs) denoted as V-LVDT (Fig. 2), placed in the middle height of the specimen on two opposite sides to enable elimination of the effect of specimen bending. On both sides, the LVDTs were combined by extra displacement transducers of different resolutions to test their performance and provide most accurate measurements. Lateral strains (ε_H) were measured by another pair of horizontal LVDTs (H-LVDT on Fig. 2), also placed in the middle height of the specimen. Conventional LVDTs were glued directly on the rubber membrane and fit very well between the large grains (see Fig. 2). Due to the large size of the specimen no correction for the effect of membrane force was applied in the analysis of the test results.

Testing program

The specimen was subjected to three load sequences as shown in Fig. 3a representing the expected condition of use of lightweight material as vibration-reducing material. Considering three possible locations of its use, the material was consolidated to three confinement pressures, p′ = 5 kPa, 25 kPa and 40 kPa. These values were selected to represent stresses in the material used in trenches alongside railway tracks as vibration countermeasure and fill/embankment material under railway tracks and vibration-reducing pads under high-frequency vibrating machinery. Every load sequence consists of 6 load phases: (1) consolidation, (2) monotonic compression, (3) small strain unloading-reloading cycles, (4) large unloading-reloading cycles (i.e. cyclic loading), (5) small strain unloading-reloading cycles, and (6) complete unloading. The loading parameters in each load phase are described in Table 2.

Every load sequence starts with consolidation (load phase 1) at defined confining pressure. It was followed by the monotonic compression loading (load phase 2), and 50 cycles of cyclic loading (load phase 4) to represent, in a simple manner, the gradual natural compaction of the material. Besides those large unloading-reloading cycles simulating cyclic loading with complete unloading, there were also approximately five small unloading-reloading cycles conducted before (load phase 3) and after (load phase 5) cyclic loading (load phase 4). These were load cycles at very small strain range. The objective was to enable evaluation of equivalent linear behaviour of the material. Each sequence was finished with unloading.

The tests were performed in stress controlled mode, with loading rates 1 kPa/min in loading phases 1, 2 and 6. During small unloading-reloading cycles (load phases 3 and 5) loading rates were decreased to 0.1 kPa/min, while during load phase 4, it was set to 0.1, 0.6 and 2 kPa/s for load sequences 1, 2 and 3, respectively.

Test results

Three load sequences with detailed stress-strain response of tested specimens are presented in Fig. 3b–d. The loading phase 1 in load sequence 1 (Fig. 3b) started already during the specimen preparation phase as some confinement was needed when the moulding frame was removed. Thus, displacement transducers were installed in the latter phase of consolidation (displacement measurements from consolidation phase are not shown on Fig. 3b).

As the test was conducted in triaxial mode, shear stress, τ, and shear strain, γ, were respectively calculated as $\tau = (\sigma_1 - \sigma_3)/2$ and $\gamma_{av,L} = \varepsilon_{v,av} - \varepsilon_{H,av}$. The index “av” denotes that the strain was averaged from strains measured on two opposite sides of the test specimen, and “L” indicated that it was measured locally, i.e. directly on the specimen to eliminate errors such as bedding error.

One can observe clear hysteresis response of the specimen during large load cycles at low confining pressure (Fig. 3b), which decreases

Table 2
Loading parameters during the test.

Load sequence	Loading phase	Confining pressure, p′ (kPa)	Control parameter	Number of load cycles	Aim of loading
1	1	5	p′ from 0 to 5 kPa	1	Consolidation
	2	5	q from 0 to 0.5 kPa	1	Monotonic compression
	3	5	ε_v ± 0.001%	5	Quasi-elastic response
	4	5	q = 0.5–0–0.5 kPa	50	Cyclic loading
	5	5	ε_v ± 0.001%	5	Quasi-elastic response
	6	5	q from 0.5 to 0 kPa	1	Unloading
2	1	25	p′ from 0 to 25 kPa	1	Consolidation
	2	25	q from 0 to 1.0 kPa	1	Monotonic compression
	3	25	ε_v ± 0.001%	5	Quasi-elastic response
	4	25	q = 1.0–0–1.0 kPa	50	Cyclic loading
	5	25	ε_v ± 0.001%	5	Quasi-elastic response
	6	25	q from 0.5 to 0 kPa	1	Unloading
3	1	40	p′ from 0 to 40 kPa	1	Consolidation
	2	40	q from 0 to 10 kPa	1	Monotonic compression
	3	40	ε_v ± 0.001%	5	Quasi-elastic response
	4	40	q = 10–0–10 kPa	50	Cyclic loading
	5	40	ε_v ± 0.001%	5	Quasi-elastic response
	6	40	q from 10 to 0 kPa	1	Unloading

q = deviatoric stress, $q = \sigma_1 - \sigma_3$.
p′ = confining pressure, $p' = (\sigma_1 + 2\sigma_3)/3$.
ε_v = vertical (axial) strain.

with higher confinement. On the other hand, prominent creeping affects occurs at higher confining pressure (Fig. 3c and d) causing particular difficulties in evaluation of readings during loading phases 3 and 5.

Quasi-elastic (equivalent linear) response of the specimen was planned to be evaluated from stress-strain measurements during loading phases 3 and 5. Therefore, extremely small amplitude load cycles at axial strain range up to $\varepsilon_v = \pm 0.001\%$ were applied to evaluate secant modulus within the elastic response. Due to the creeping affects this approach was not possible at higher confining pressures, but enables comparison of two shear modulus evaluation approaches.

Analysis of test results

Shear modulus and variation

Secant shear modulus and its dependency on strain level was further evaluated from the initial (virgin) monotonic compression load curve (loading phase 2) and monotonic compression load curve after 50 load cycles (loading phase 4). High resolutions of deformation transducers installed locally on specimen and inner load cell enabled evaluation of shear modulus at very small strain range. Fig. 4 shows very good match of the results evaluated from monotonic compression load curves with those evaluated on the basis of small amplitude load cycles (loading phase 3) that prove the concept of evaluation. Thus, secant shear modulus was further evaluated for different values of shear strain during the monotonic compression.

Secant shear modulus and its reduction with shear strain were further compared for confining pressures 5 kPa, 25 kPa and 40 kPa and for different load phases (2 and 4), and the results are presented on Fig. 5. It can be observed from the figure that cyclic loading causes an increase of specimen stiffness. This could be expected as the specimen was prepared with light compaction, hence, some compaction should be expected due to cyclic loading. As is evident in Fig. 3b–d, this compaction is executed in the first few cycles and the shapes of stress-strain curves remain almost the same in the later phases of cyclic loading.

As the present research is focused on cyclically loaded applications, plots of secant shear moduli as functions of shear strain evaluated from the shear stress-shear strain curves after 50 load cycles are further considered. The results display the expected trend of reduction of shear

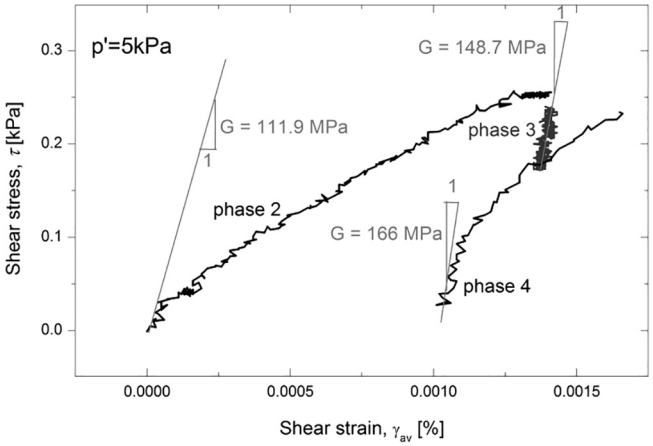

Fig. 4. Comparison of secant shear modulus evaluated from virgin monotonic loading (phase 2), monotonic loading in 50th cycle (phase 4) and shear modulus from typical small strain unloading-reloading cycle before large cyclic loading (phase 3) at confining pressure $p' = 5$ kPa.

modulus with shear strain. Values of the initial shear modulus, G_{max}, were read out of the secant shear modulus degradation curves at very small strain levels (about 10^{-4}%) for various confining pressures. Fig. 6 shows the shear modulus reduction curves, computed from normalization of the shear moduli by G_{max}, as function of shear strain for the three confining pressures. The elastic threshold shear strain at which the non-linear behaviour is observed, seems dependent on the confining pressure, and it ranges from $\gamma \approx 10^{-5}$% for confining pressure p′ = 5 kPa to $\gamma \approx 10^{-4}$% for confining pressure p′ = 40 kPa. Fig. 6 also displays the results obtained for ballast by Dyvik and Kaynia [8] using cylindrical vacuum triaxial tests and the reduction curves for sand/gravel proposed by Menq [27] for the same particle size and C_u as those tested in the present study. From these results, it is evident that foamed glass exhibits significantly larger modulus reduction compared to natural sand/gravel and ballast. It is expected that this characteristics strongly depends on the method of fabrication of these lightweight products and should therefore be evaluated with dedicated tests.

The large reduction of the shear modulus at early stage of loading can be highlighted by further examination of the monotonic compression curves in Fig. 4. The figure clearly shows the very short initial

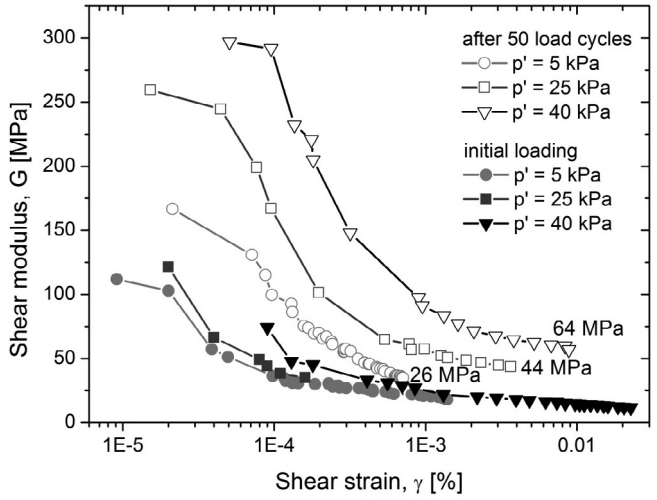

Fig. 5. Secant shear modulus vs. shear strain from virgin stress-strain curve (initial loading, phase 2) and from stress-strain curve after 50 load cycles (phase 4) for three confining pressures.

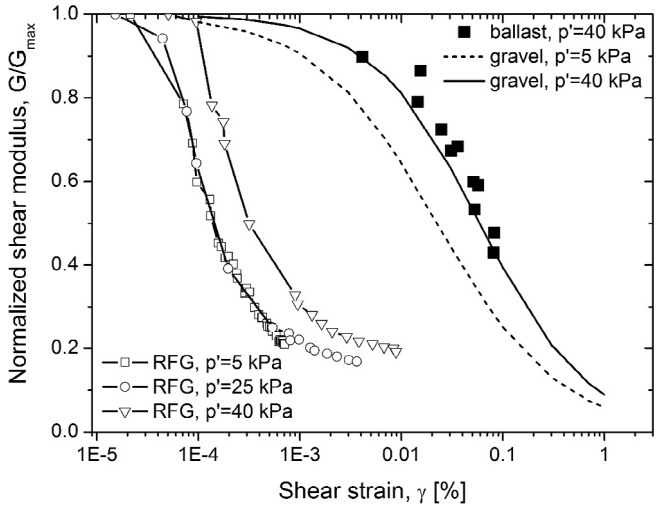

Fig. 6. Normalized shear modulus of tested recycled foamed glass (RFG) as a function of shear strain and comparison with data from other sources.

elastic parts with very high stiffnesses. The initial shear modulus, G_{max}, was evaluated from this region. However, this region lasts over a very small strain range ($\gamma < 10^{-3}$% for p′ = 5 kPa) and it further shrinks with an increase of confinement; therefore, G_{max} (as evaluated above) is not applicable to most dynamic/vibration problems in geotechnics. On the other hand, the monotonic compression curve transfers into a sustained nearly linear response with lower stiffness at the end of the initial short region. As the stress/strain range applied during this second part of the stress-strain curve correspond to loading conditions expected in many vibration-related applications, this study has focused in the following on the cyclic behaviour in this region of response. This region is referred to quasi-elastic region with the corresponding shear modulus referred to as G_0 in the following.

Fig. 7a–c presents a closer look at the monotonic compression curves after 50 load cycles for three confining pressures. The quasi-elastic initial shear modulus, were evaluated from the second elastic part of those curves for various confining pressures, and they were compared with the results of other studies on crushed rocks and gravel (e.g. [34,18,32,36,11]). Prange [34] performed resonant column tests on ballast with D_{50} = 40 mm, the results of which are relevant to the tests performed in the present study. Kokusho and Esashi [18] performed triaxial tests on both crushed rock with D_{50} = 30 mm and round

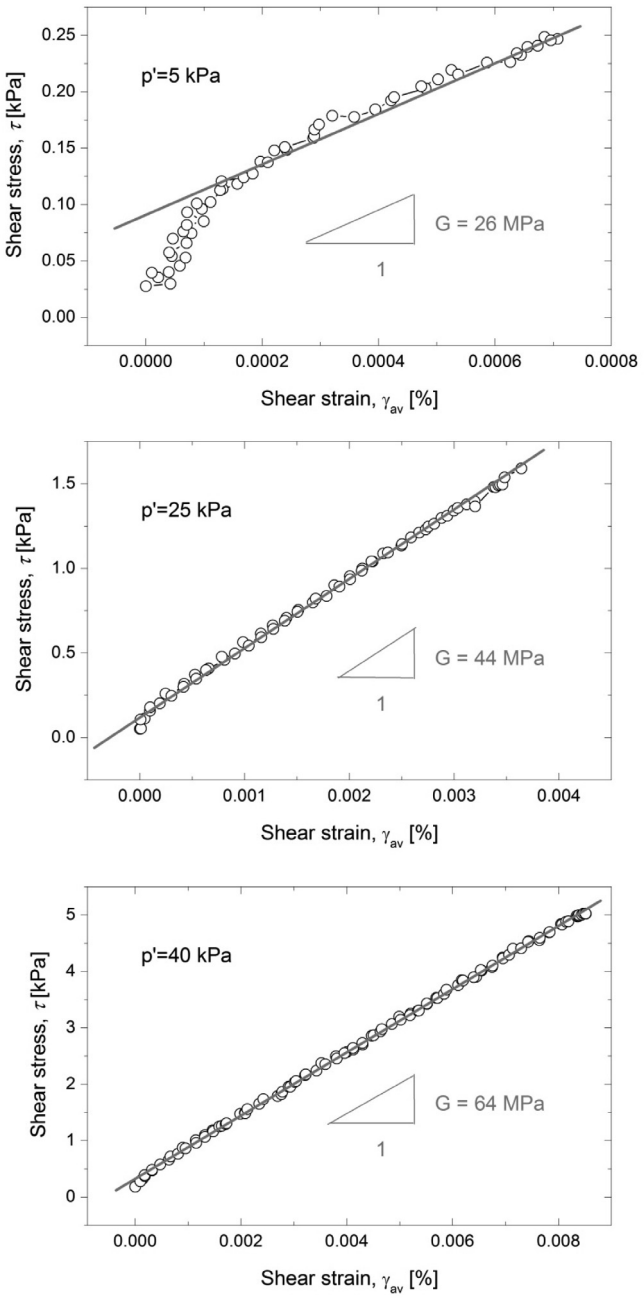

Fig. 7. Quasi-elastic initial shear modulus, G_0 evaluated for the branch following the initial elastic phase during monotonic compression curves after 50 load cycles for three confining pressures.

gravel with D_{50} = 10 mm. Nishio et al. [32] performed triaxial tests on undisturbed gravel with D_{50} = 10 mm. As in most previous studies, the general form of expression $G_0 = A\,F(e)\,(p')^n$ [41] was used to describe a relationship between initial shear modulus, G_0, and confining pressure, p′. In this expression, *e* is the void ratio, F(e) is a term that describes the effect of void ratio, and the parameters *A* and *n* are chosen for best fitting of the data. Using the measured values, the quasi-elastic shear modulus of foamed glass aggregate was found to be best described by Eq. (1)

$$G_0 = 7000 \times \frac{(2.17 - e)^2}{1 + e} \times (p')^{0.4} \quad (1)$$

The values of G_0 computed by the above-mentioned empirical expressions for different coarse-grained materials are compared in Fig. 8

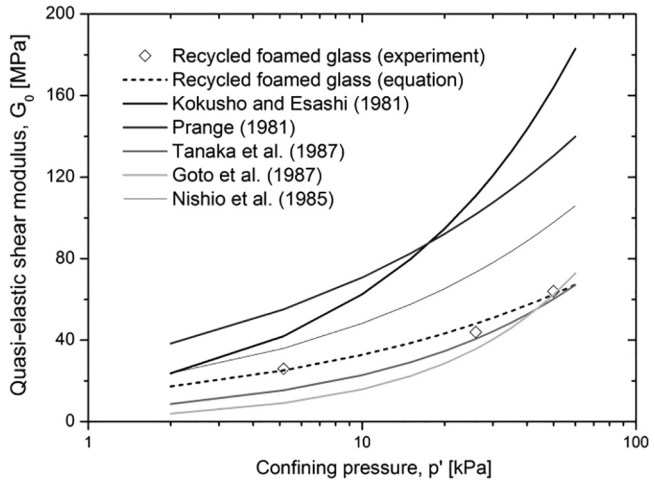

Fig. 8. Comparison of quasi-elastic shear modulus, G_0 of the foamed glass aggregate with the values of initial shear modulus of other coarse-grained materials.

with the values measured for the foamed glass aggregate. The data indicate that G_0 of foamed glass is similar of slightly lower magnitude than other materials, it is closest to the data for gravel proposed by Tanaka et al. [36] and Nishio et al. [32]. Like other coarse-grained materials, foamed glass aggregate exhibits high dependence of the quasi-elastic shear modulus on confining pressure.

Damping

Because cyclic loading was conducted using only one stress amplitude in each load sequence, it was possible to compute the damping ratio *D* in each load sequence only at one strain level. Fig. 9a–c present hysteresis loops at the end of cyclic loading for the three confining pressures considered in this study. The damping ratios were evaluated from the area of the stress-strain loops (dissipated energy) and the maximum strain energy [19]. The damping values computed for the confining pressures 5 kPa, 25 kPa and 40 kPa were calculated at about 9%, 3.3% and 3.2%, respectively. It should be noticed that these damping values are for one-way loading, as shown in the figure, and may not be directly comparable with the traditional damping ratios computed for two-way symmetrical loading. Except for the results for the lowest confining pressure (5 kPa), which appear to be affected by the low confining pressure, the computed damping ratios provide reasonable values for their representative shear strains. If one takes into consideration a representative shear strain based on the secant stiffness through the two ends of the hysteresis curves, one could compute the shear strains of about 0.003% and 0.007% for the confining pressures 25 kPa and 40 kPa, respectively. The computed damping ratios (3.3% and 3.2%) are generally in the expected range based on the published data. Although compared at different (but still very small) strain values, the dependency of the damping ratio to the confining pressure can be described by the formula indicated in Fig. 10. It should be noted that this formula can be applied for the small strain range of response.

Discussion

Results presented in the preceding section might indicate unusual deformation behaviour of foamed glass aggregate. As strains and loads were measured locally by very accurate and calibrated devices and the test results were validated by test repetitions, it can be concluded that results present the actual material response. High initial stiffness, small elastic threshold strain and significant modulus reduction compared to other granular materials point to the brittle structure of the tested material. The deformation characteristics and its dependence on

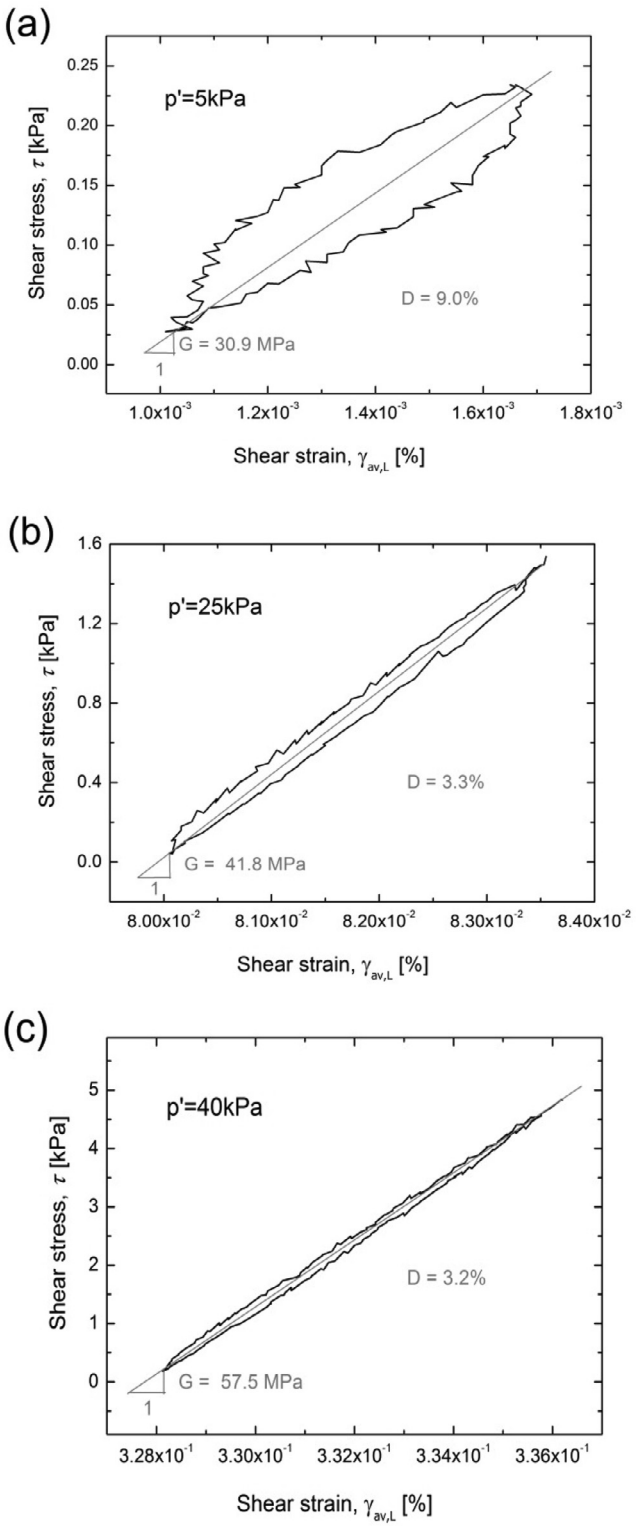

Fig. 9. Relationship between shear stress-shear strain during 50th load-unload cycle at confining pressures; (a) $p' = 5$ kPa, (b) $p' = 25$ kPa, and (c) $p' = 40$ kPa.

confining pressure can be explained by considering the grain's cellular structure. When exposed to pressure, the fragile cellular structure near the surface crush and the turn into powder (Fig. 11). The effect is observed at low confining pressure (shallow depth) and it causes permanent deformation and material change at the contact points between the grains. Thus, significant decrease of damping ratio and an increase of elastic threshold strain with an increase of confining pressure might be

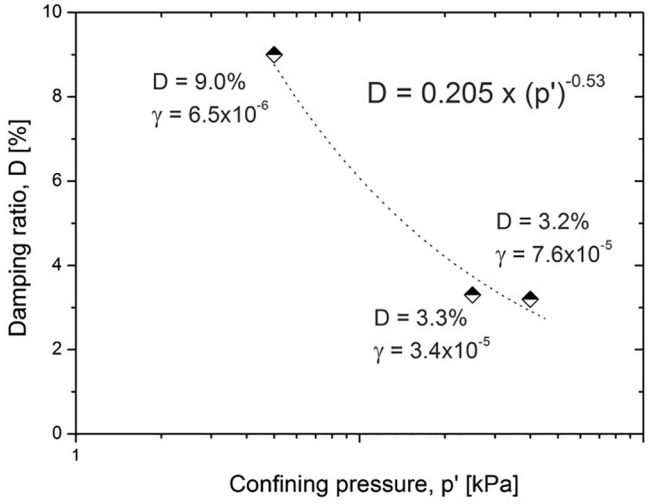

Fig. 10. Damping ratio vs. confining pressure after 50 load cycles.

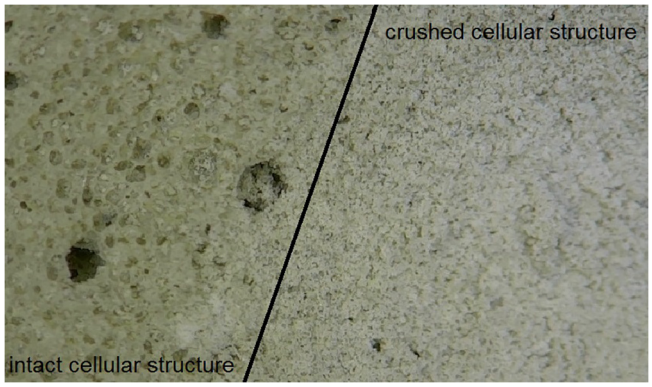

Fig. 11. Foamed glass grain microstructure magnified with digital microscope: (left) virgin surface; (right) surface exposed to load.

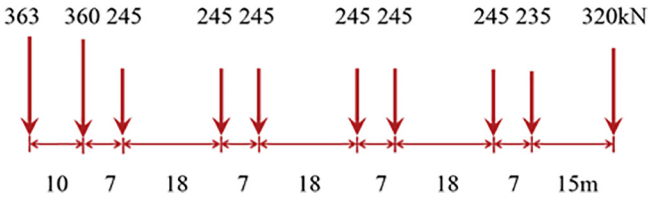

Fig. 12. Bogie loads of X2000 train used in *VibTrain* simulations.

explained by surface micro-structure changes of foamed glass grains when intergranular pressure is increased. This part of response corresponds to the initial very short elastic part of stress-strain curve. This effect was more prominent during p′ = 5 kPa as the material was initially intact (no grain surface damages). During the tests at higher confining pressures, the contact surfaces are already damaged and crushing of cellular structure happen deeper and are less prominent.

Moreover, as stated earlier, longer elastic part of the stress-strain curve follows after the initial crushing of the surface cellular structure. This quasi-elastic part of the stress-strain curve corresponds to expected conditions of the use of most material as vibration-reducing material in different geotechnical applications. One such application is presented in the next section.

Effect of lightweight material on railway vibration

This section evaluates the influence of lightweight material on railway vibration. To qualify for usage as the main material for railway track construction, more tests similar to those specified for ballasts, including among others the Los Angeles abrasion test, are required. Evaluation of suitability of foamed glass for railway tracks is outside of the scope of this paper. The intention of the simulations performed in this section is only to explore numerically the impact of the stiffness and light mass of this material on track vibration. The findings of this study can be extended to other lightweight materials independent of their suitability as high load bearing material. If proved to be suitable for railway applications, lightweight material has the potential of being used as for example fill and embankments under the tracks.

Numerical simulation tool

The computational tool *VibTrain* was used to investigate the effect of replacing ballast with the lightweight material tested in this study. The ground model in *VibTrain* consists of visco-elastic soil layers over a half-space and the substructure and tracks are modelled as separate beams with elastic elements between them to represent rail/sleeper pad flexibility. The interaction between the substructure beam and the ground is accounted for by use of Green's functions for layered media developed by Kausel and Roesset [16]. The computation tool was validated against field test data at the Swedish test site Ledsgaard and for Swedish train X2000 [15]. Fig. 12 shows the bogie loads used in the simulation. While it is possible with this tool to use the axle loads in the simulations, it was decided to use the bogie loads for simplifications. Table 3 summarizes the dynamic soil parameters established for the test site at Ledsgaard using a combination of geotechnical site investigation and lab testing (see [15;23] for details). The presence of a 1.5 m peat layer at about 3.0 m depth has resulted in a low critical velocity at this site (about 200 km/h). The two profiles of shear wave velocities for the low train speed and high speed (critical speed range) were established based on a consideration of the soil nonlinearity for the two speed regimes [15].

Numerical results

Fig. 13a presents the computed track vibrations for train speeds 100, 140 and 200 and 250 km/h for the in-situ track with regular ballast. The plots in the figure clearly show the increase of track vibrations with train speed. An amplification of 10 is observed between the peak velocities as the train approaches the critical speed and beyond.

Table 3
Soil parameters applied to FE simulation of track vibration.

Soil layer	Thickness [m]	Density [kg/m^3]	V_S [m/s]		V_P [m/s]	
			V = 70 [km/h]	V = 200 [km/h]	V = 70 [km/h]	V = 200 [km/h]
Crust	1.1	1500	72	65	500	500
Organic clay	3.0	1260	41	33	500	500
Clay	4.5	1475	65	60	1500	1500
Clay	6.0	1475	87	85	1500	1500
Half space	–	1475	100	100	1500	1500

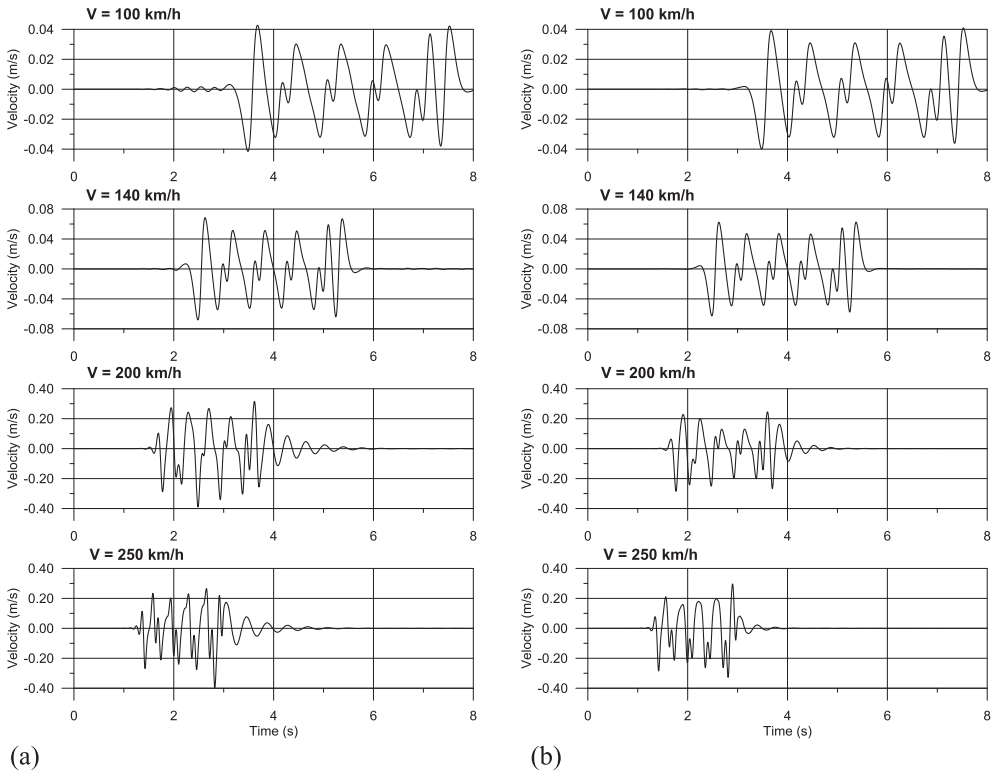

Fig. 13. Track vibrations under low and high train speeds with track/ground model at Ledsgård – (a) in-situ track, (b) track with fill/embankment replaced by lightweight aggregates.

Fig. 13b displays the corresponding results for the case in which the fill/embankment is replaced by the lightweight material. This was made by simply keeping the same track stiffness (in view of the stiffness parameters derived in previous chapters), and reducing the track mass by 50% accounting for the difference in the mass of the fill and lightweight material. The plots in this figure show that at low train speeds, the two responses are practically identical (with the results for lightweight track only slightly lower). This result is as expected because the track/ground response is practically quasi-static for speeds way below the critical speed [15]. However, at the speeds in the critical speed regime (200 and 250 km/h), the dynamics of the track have larger roles. This is manifested by the clearly lower responses of the track with lightweight material. This is a useful observation which most likely applies to all types of lightweight materials.

Conclusion

Deformation properties of lightweight coarse grained material from recycled foamed glass have been tested. The attention centered particularly on stiffness and damping properties of the tested material. Large-scale triaxial tests with monotonic and cyclic loading at small to medium strain ranges were conducted. Three load sequences, representing the expected condition of use of lightweight material as vibration-reducing material, have been considered. The results indicate that the elastic threshold shear strain and damping ratio are strongly dependent on confining pressure. Noticeable initial increase of stiffness during cyclic loading was recognized, which is caused by additional material compaction in first load cycles due to light compaction preparation of test specimens.

Brittle cellular structure of lightweight foamed glass causes two stage deformation behaviour of material, with high initial stiffness, small elastic threshold strain and significant modulus reduction compared to other kind of natural materials in the first stage. The first stage of deformation behaviour is governed by crushing of material cellular structure near the surface of grains due to the increase of intergranular pressure. The second stage of material nearly linear elastic deformation behaviour is longer and presents expected conditions of the use of lightweight material as vibration-reducing material in railway applications. Quasi-elastic shear moduli, G_0, measured at different confining pressures seem to generally follow the empirical expressions proposed in the literature for gravel and ballast. A new expression, with similar form as those in the literature, has been proposed in this study for the foamed glass. Damping in small strain range has been evaluated as well.

Finally, the impact of replacing the fill/embankment under the railway track with lightweight material has been analysed in the paper. The results of the numerical simulations show that lightweight materials tend to slightly reduce the track vibration in the critical speed range.

Acknowledgements

The authors would like to acknowledge the support for this study by the research project DESTination Rail - Decision Support Tool for Rail Infrastructure Managers, funded by the European Commission, Grant Agreement 636285 (H2020-MG-2014-2015). The authors are also thankful to Mr. Thomas Bjørhusdal for his cooperation and providing samples of Glasopor for this research.

References

[1] AnhDan LQ, Tatsuoka F, Koseki J. Viscous effects on the stress-strain behavior of gravelly soil in drained triaxial compression. Geotech Test J 2006;29(4):330–40.
[4] Arulrajah A, Disfani MM, Maghoolpilehrood F, Horpibulsuk S, Udonchai A, Imteaz M, et al. Engineering and environmental properties of foamed recycled glass as a lightweight engineering material. J Cleaner Prod 2015;94:369–75.
[5] Ayati B, Ferrándiz-Mas V, Newport D, Cheeseman C. Use of clay in the manufacture of lightweight aggregate. Constr Build Mater 2018;162:124–31.
[6] Beinbrech G, Hillmann R. EPS in road construction—Current situation in Germany. Geotext Geomembr 1997;15(1–3):39–57.
[7] Bush AL. Lightweight aggregates. United States Min Resour, Geol Surv Prof Paper 1973;820:333–56.
[8] Dyvik R, Kaynia AM. Large-scale triaxial tests on railway embankment material, railroad ballast testing and properties, ASTM STP1605. West Conshohocken, PA: ASTM International; 2018. p. 163–80.
[9] EPD. Environmental Product Declaration, Glasopor 10-60 (Cellular glass aggregate), NEPD-1243-396-EN, www.epd-norge.no; 2017.

[10] Farnsworth CB, Bartlett SF, Negussey D, Stuedlein AW. Rapid construction and settlement behavior of embankment systems on soft foundation soils. J Geotech Geoenviron Eng 2008;134(3).
[11] Goto S, Syamoto Y, Tamaoki S. Dynamics properties of undisturbed gravel samples obtained by the in situ freezing method. Proceedings of the 8th Asian Regional Conference on Soil Mechanics and Foundation Engineering. Kyoto; 1987.
[12] Huang J, Su Q, Zhao W, Li T, Zhang X. Experimental study on use of lightweight foam concrete as subgrade bed filler of ballastless track. Constr Build Mater 2017;149:911–20.
[13] Øiseth E, Aabøe R, Hoff I. Field test comparing frost insulation materials in road construction. In: 13th international conference on cold regions; 2006.
[15] Kaynia AM, Madshus C, Zackrisson P. Ground vibration from high speed tains: prediction and countermeasure. J Geotech & Geoenv Engrg, ASCE 2000;126(6):531–7.
[16] Kausel E, Roesset JM. Stiffness matrices for layered soils. Bull Seism Soc Am 1981;71(6):1743–61.
[17] Kurauchi T, Sato N, Kamigaito O, Komatsu N. Mechanism of high energy absorption by foamed materials-foamed rigid polyurethane and foamed glass. J Mater Sci 1984;19(3):871–80.
[18] Kokusho T, Esashi Y. Cyclic triaxial test on sands and coarse materials. Proceedings of the 10th international conference on soil mechanics and foundation engineering Stockholm, Sweden, vol. 1. Rotterdam, The Netherlands: A. A. Balkema; 1981. p. 673–6.
[19] Kramer SL. Geotechnical earthquake engineering. Prentice Hall; 1996. p. 653.
[20] Lenart S, Koseki J, Miyashita Y, Sato T. Large-scale triaxial tests of dense gravel material at low confining pressures. Soils Found 2014;54(1):45–55.
[21] Loranger B, Kuznetsova E, Hoff I, Aksnes J, Skoglund KA. Evaluation of Norwegian gradation based regulation for frost susceptibility of crushed rock aggregates in roads and railways. In: Loizoseditor. Bearing capacity of roads, railways and airfields. Taylor & Francis Group; 2017. p. 2077–85.
[22] Lu J, Onitsuka K. Construction utilization of foamed waste glass. J Environ Sci 2004;16(2):302–7.
[23] Madshus C, Kaynia AM. High-speed railway lines on soft ground: dynamic behaviour at critical train speed. J Sound Vibrat 2000;231(3):689–701.
[24] Marradi A, Pinori U, Betti G. The use of lightweight materials in road embankment construction. Proc - Soc Behav Sci 2012;53:1000–9.
[25] Maqbool S, Koseki J. Large-scale triaxial tests to study effects of compaction energy and large cyclic load-ing history on shear behavior of gravel. Soils Found 2010;50(5):633–44.
[26] Masad E, Taha R, Ho C, Papagiannakis T. Engineering properties of tire/soil mixtures as a lightweight fill material. Geotech Test J 1996;19(3):297–304.
[27] Menq F. Dynamic properties of sandy and gravelly soils PhD dissertation Univ. of Texas at Austin; 2003.
[28] Mohajerani A, Ashdown M, Abdihashi L, Nazem M. Expanded polystyrene geofoam in pavement construction. Constr Build Mater 2017;157:438–48.
[29] Mohajerani A, Vajna J, Cheung THH, Kurmus H, Arulrajah A, Horpibulsuk S. Practical recycling applications of crushed waste glass in construction materials: a review. Constr Build Mater 2017;156:443–67.
[30] Morgan JS, Wood JL, Bradt RC. Cell size effects on the strength of foamed glass. Mater Sci Eng 1981;47(1):37–42.
[31] Nakhaei A, Marandi SM, Sani Kermani S, Bagheripour MH. Dynamic properties of granular soils mixed with granulated rubber. Soil Dyn Earthquake Eng 2012;43:124–32.
[32] Nishio N, Tamaoki K, Machida Y. Dynamic deformation characteristics of crushed gravel by means of large-size triaxial test apparatus. Proceedings of the 20th annual convention, Japanese society of soil mechanics and foundation engineering, Tokyo, Japan. 1985. p. 603–4.
[33] Pierce CE, Blackwell MC. Potential of scrap tire rubber as lightweight aggregate in flowable fill. Waste Manage 2003;23(3):197–208.
[34] Prange B. Resonant Column Testing of Railroad Ballast. Proceedings of the 10th international conference on soil mechanics and foundation engineering, Stockholm, Sweden, Vol. 3. Rotterdam, The Netherlands: A. A. Balkema; 1981. p. 273–82.
[35] Sevi AF, Ge L, Take WA. A large-scale triaxial apparatus for prototype railroad ballast testing. Geotech Test J 2009;32(4):297–304.
[36] Tanaka Y, Kudo K, Yoshida Y, Ikemi M. A study on the mechanical properties of sandy gravel-Dynamic properties of reconstituted sample. Research report No. U87019. Abiko, Japan; Central Research Institute of Electric Power Industry; 1987 [in Japanese].
[37] Volland S, Kazmina O, Vereshchagin V, Dushkina M. Recycling of sand sludge as a resource for lightweight aggregates. Constr Build Mater 2014;52:361–5.
[38] Watn A. Lightweight aggregates for civil engineering. Technical solutions, mechanical properties, certification and quality control, Research Projects by SINTEF; 2008. p. 20.
[39] Wang S, Gao Y. Laboratory test study on dynamic deformation characteristics of EPS block. Rock Soil Mech, CNKI J 2006;2006(10).
[40] Zhang X, Zeng Z. Application of eco-friendly material—foamed glass. J Build Mater, CNKI J 2006;2006(2).
[41] Hardin BO. The nature of stress-strain behavior of soils. In: Proc. Earthquake Engineering and Soil Dynamics Conference, Pasadena, 1978, ASCE, V.I, pp. 3–90.